JACS
JOURNAL OF THE AMERICAN CHEMICAL SOCIETY

Article

pubs.acs.org/JACS

Modulating Paratropicity Strength in Diareno-Fused Antiaromatics

Conerd K. Frederickson,[†] Lev N. Zakharov,[‡] and Michael M. Haley*[,†]

[†]Department of Chemistry & Biochemistry and the Materials Science Institute, University of Oregon, Eugene, Oregon 97403-1253, United States

[‡]CAMCOR, University of Oregon, Eugene, Oregon 97403-1433, United States

Supporting Information

ABSTRACT: Understanding and controlling the electronic structure of molecules is crucial when designing and optimizing new organic semiconductor materials. We report the regioselective synthesis of eight π-expanded diarenoindacene analogues based on the indeno[1,2-*b*]fluorene framework along with the computational investigation of an array of diareno-fused antiaromatic compounds possessing *s*-indacene, pentalene, or cyclobutadiene cores. Analysis of the experimental and computationally derived optoelectronic properties uncovered a linear correlation between the bond order of the fused arene bond and the paratropicity strength of the antiaromatic unit. The E^1_{red} for the pentalene and indacene core molecules correlates well with their calculated $NICS_{\pi ZZ}$ values. The findings of this study can be used to predict the properties of, and thus rationally design, new diareno-fused antiaromatic molecules for use as organic semiconductors.

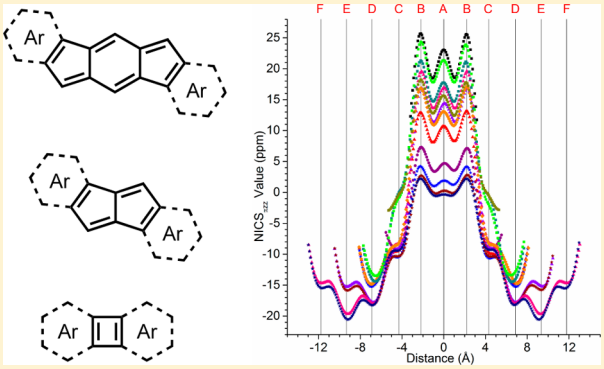

INTRODUCTION

Aromaticity has long held the interest of theoretical chemists and synthetic chemists alike.[1−5] Even before Hückel codified the $(4n+2)$ π-electron rule for monocyclic systems in 1931,[5] significant work investigating aromatic properties had been performed in the late 19th and early 20th centuries via examination of benzene, thiophene and other simple aromatic compounds.[4,6−9] Although predicted by Hückel,[5] it was not until 1967 that Breslow and co-workers proposed the concept of antiaromaticity as the inverse of aromaticity, where cyclic conjugation of $(4n)$ π-electrons leads to a destabilization compared to a suitable reference.[10,11] Several groups have pushed the study of antiaromaticity forward,[12−18] and cohesive descriptions of the properties of aromatic and antiaromatic molecules have been advanced by Breslow,[11] Wiberg,[9] and Krygowski.[1] Despite a significant amount of theoretical study and increasing interest in their application as organic semiconductors,[15,19−22] examples of synthetic control over the antiaromatic properties of a molecular framework remain quite rare.

Research into polycyclic conjugated hydrocarbons (PCHs) has expanded rapidly over the last two decades, with the emergence of the organic electronics industry and a desire to produce new functional materials that are not based on inorganic solids.[23−29] The rigid, highly conjugated structures and optoelectronic properties of PCHs (e.g., acenes) made them an early target of interest as organic semiconductors;[29−33] however, the properties that make acenes desirable also impart an inherent instability: many longer acenes are known to photooxidize and/or dimerize readily under ambient conditions unless sufficiently stabilized.[32,34,35] With these problems in mind, there has been a push to develop acene alternatives that can replicate the promising electronic properties without the instability of these molecules.[36−40]

One method of developing materials with the potential to produce devices with high charge carrier mobility is to reduce the aromaticity of a compound while retaining comparable conjugation length. This can be accomplished by replacing some of the six-membered rings with five-membered heterocyclic rings (e.g., anthradithiophenes (**1**),[41−43] dibenzothienothiophenes (**2**),[44,45] Figure 1). Alternatively, introduction of five-membered, fully conjugated carbocyclic rings (e.g., dibenzopentalenes (**3**),[46−48] indeno[1,2-*b*]fluorenes ([1,2-*b*]IF **4**))[49−51] affords diareno-fused antiaromatic compounds. Both classes of five-membered ring molecules are of special interest as evidence suggests that reduced aromaticity or, in particular, pronounced antiaromaticity have the potential to increase molecular conductivity.[19,21,52,53] Recent work on the diareno-fused pentalenes has expanded these molecules beyond simple dibenzopentalenes (e.g., **3**) to dinaphthopentalene (e.g., **5**, **6**) and dianthracenopentalene derivatives.[46,47,54,55] The extension of the outer ring introduces different structural isomers and the possibility of isomer dependent properties; in fact, the dinaphthopentalene isomers **5** and **6** prepared by Kawase's group showed significant differences in both optical and electronic properties.[47] Such differences were also predicted computationally for the 1,4-diazapentalenes[56] and observed in

Received: November 2, 2016
Published: December 1, 2016

DOI: 10.1021/jacs.6b11397
J. Am. Chem. Soc. 2016, 138, 16827−16838

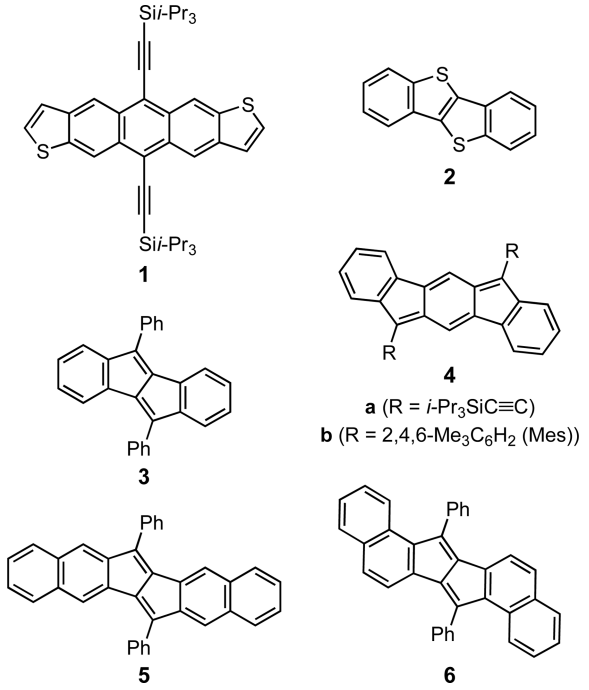

Figure 1. Literature examples of five-membered ring PCHs such as *anti*-anthradithiophene (**1**), dibenzothienothiophene (**2**), dibenzopentalene (**3**), indeno[1,2-*b*]fluorene (**4**), *linear*-dinaphthopentalene (**5**), and *anti*-dinaphthopentalene (**6**).

monoarenopentalenes by Nakamura.[57] Although the inclusion of antiaromatic rings within large polycyclic systems shows potential for the development of new functional organic electronic materials, there has yet to be detailed examination of how the conflicting ring currents interact, and thus influence, semiconductor properties in diareno-fused antiaromatics.[26]

We report herein the synthesis and characterization of a series of symmetric dinaphthoindacene regioisomers (**7**–**9**, Figure 2), along with the computational investigation of ring currents in diareno-fused indacenes, pentalenes and cyclobutadienes. To examine the influence of R group conjugation, we prepared both (triisopropylsilyl)ethynyl (**a**) and mesityl (**b**) derivatives. Significant differences in the properties of the three

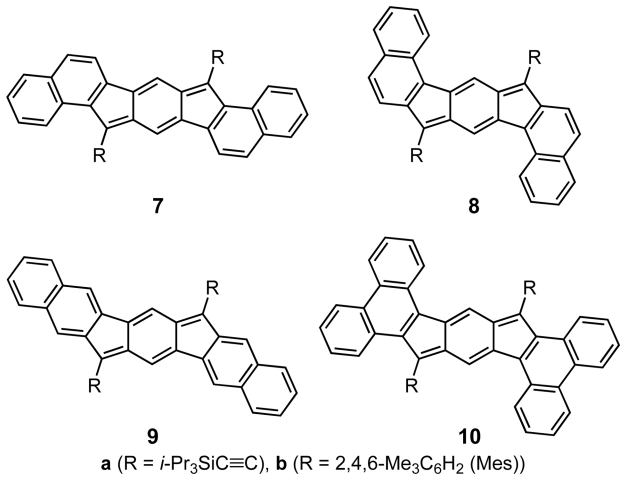

Figure 2. Target molecules *anti*-dinaphthoindacene (**7**), *syn*-dinaphthoindacene (**8**), *linear*-dinaphthoindacene (**9**), and 9,10-diphenanthroindacene (**10**).

dinaphthoindacene isomers concur with the nucleus independent chemical shift (NICS)-XY scan analysis that depicts more intense paratropic currents in the indacene core of the *anti*-(**7**) and *syn*-(**8**) dinaphthoindacene (DNI) isomers compared to the *linear*-DNI isomer (**9**). Structural comparisons reveal a trend between the bond order of the arene-indacene fused bond and the maximum NICS$_{\pi ZZ}$ value in the center ring, with a fusion bond order closer to two correlating to more positive NICS$_{\pi ZZ}$ values. Calculations performed on diarenopentalenes and diarenocyclobutadienes illustrate similar trends, suggesting this correlation may be general to all diareno-fused antiaromatic systems. To confirm this predictive power, we then prepared the analogous 9,10-diphenanthroindacenes (DPI, **10a**,**b**) and determined their optical and electronic properties. Finally, comparison of the E^1_{red} potentials to the NICS$_{\pi ZZ}$ values for the indacene and pentalene systems showed that the calculated NICS$_{\pi ZZ}$ numbers can be directly related to experimental results, with increasing paratropicity of the antiaromatic core correlating with less negative reduction potentials.[24,27,32−37]

RESULTS AND DISCUSSION

Synthesis. The initial goal of this project was to examine the effect of expanding the outer conjugation of indeno[1,2-

Scheme 1. "Inside-Out" Synthesis of Dione 11 and DNI 7a

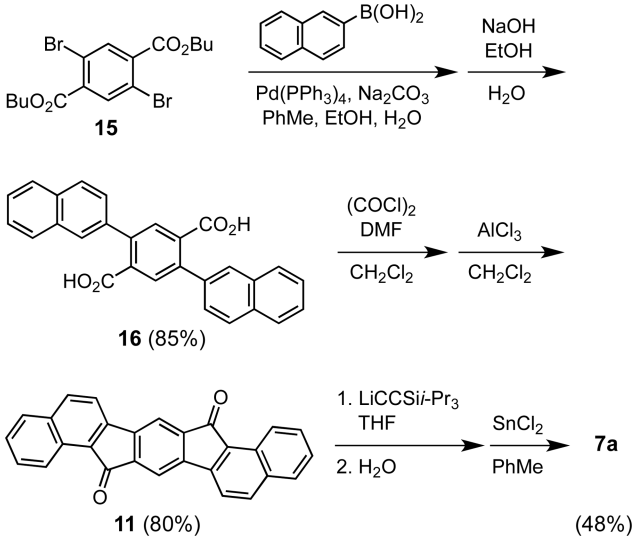

b]fluorene derivatives. To explore this quickly, we chose to exchange the outer benzene rings for naphthalenes, affording isomeric structures **7**–**9**. For these and all other diarenoindacene systems, we adopted the naming scheme utilized for the previously published indacenodibenzothiophenes.[58,59] Compound **7**, with the double bond in the first benzo fusion and the adjacent R group on opposite sides of the molecule, is referred to as *anti*-DNI, whereas compound **8** is referred to as *syn*-DNI because the R substituent and the double bond in the first benzo fusion are on the same side of the molecule. Compound **9**, with the indacene fused to the 2,3-bond of the naphthalene, is referred to as *linear*-DNI.

All three TIPS-ethynyl-substituted DNIs **7a**–**9a** (and DPI **10a**), along with mesityl DNIs **8b**–**9b**, were prepared via the standard protocol for most indenofluorene derivatives, namely nucleophile addition to a diketone precursor followed by reductive dearomatization of the intermediate diol. The diketones were synthesized in turn using either an "inside-

DOI: 10.1021/jacs.6b11397
J. Am. Chem. Soc. 2016, 138, 16827−16838

Scheme 2. "Outside-In" Synthesis of Diones 12−14, DNIs 8−9a/b and DPI 10a

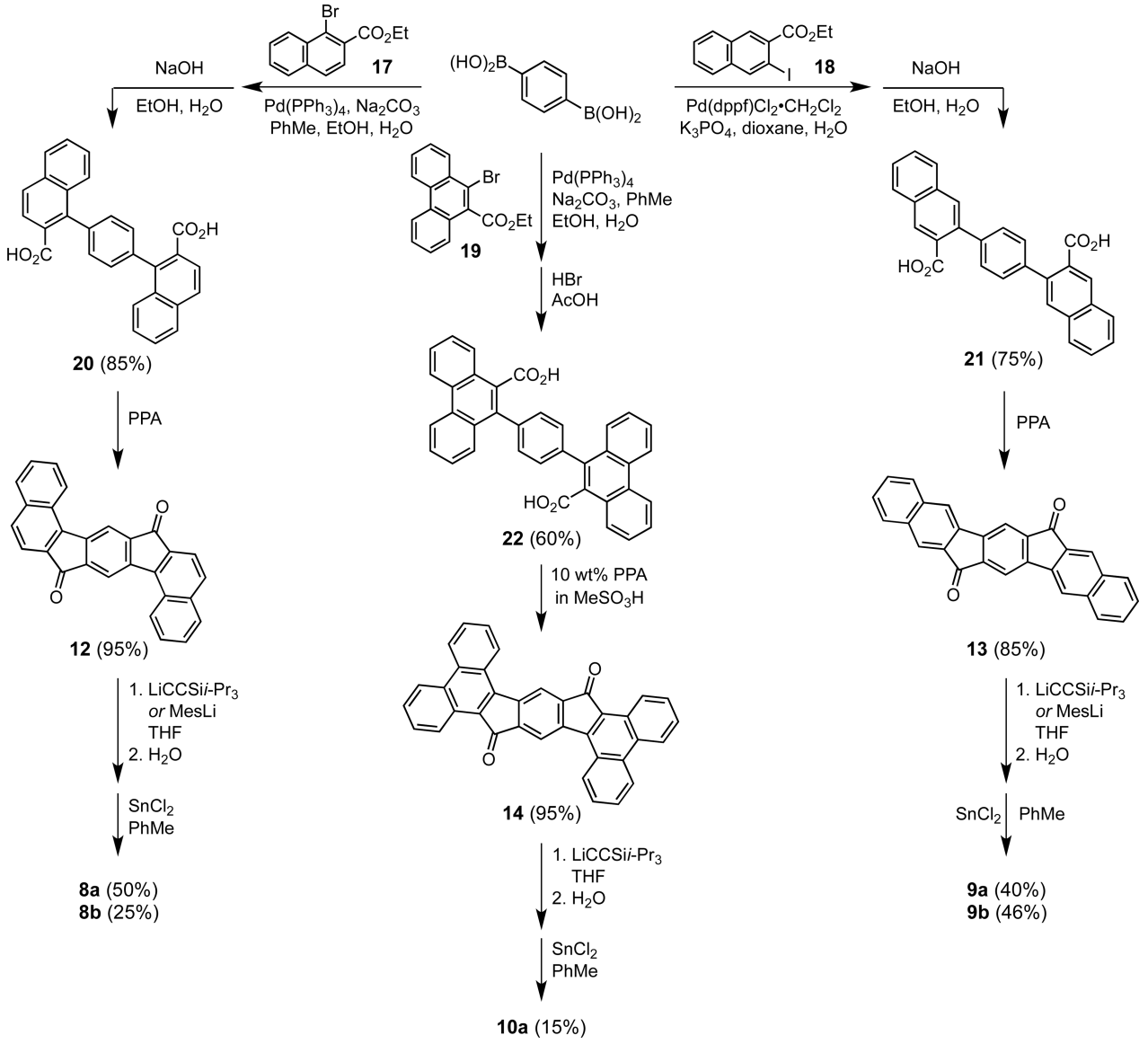

out" method, as in the case of **11**, or an "outside-in" method, for **12**-**14**. In the "inside-out" procedure (Scheme 1), dibromide **15**[60] is cross-coupled with 2-naphthaleneboronic acid under Suzuki conditions and the resulting diester saponified to give diacid **16**. Conversion to the acyl chloride with oxalyl chloride and intramolecular Friedel−Crafts acylation produced poorly soluble dione **11** in very good yield.

To avoid production of inseparable mixtures of regioisomeric diones, **12**−**14** were prepared using the "outside-in" method where the carboxylic acids are located on the outer rings and cyclize onto the central benzene ring (Scheme 2). 1,4-Phenylenediboronic acid was cross-coupled with the corresponding haloesters **17**,[61] **18**,[62] or **19**,[63] and the resultant diesters were either saponified to yield diacids **20** and **21** or exposed to more forceful conditions to afford diacid **22**. The proton NMR spectra of both **20** and **22** revealed that these molecules (as well as the corresponding esters) exist as a mixture of rotamers at room temperature, the signals of which coalesce upon heating to 70 °C. Much to our surprise, subjecting the diacids to typical Friedel−Crafts conditions such as those shown in Scheme 1, or to hot concentrated H_2SO_4, did not generate the desired ketones. Gratifyingly, switching to polyphosphoric acid (PPA) or a 10 wt % mixture of PPA in $MeSO_3H$ furnished diones **12**−**14** in excellent yield. Nucleophilic addition of either lithium (triisopropylsilyl)-acetylide to **11**−**14** or mesityllithium to **12** and **13** followed by $SnCl_2$ reduction of the intermediate diols under rigorously anaerobic conditions produced the dark blue diarenoindacenes **7a**−**10a** and **8b**−**9b** in low to moderate yields (Schemes 1 and 2).

Repeated attempts to add mesityllithium or mesitylmagnesium bromide to diones **11** and **14** either led to recovery of starting material, even at elevated temperatures, or produced intractable mixtures. This necessitated use of an alternate method to prepare **7b** and **10b**, similar to our recent synthesis of a diindenoanthracene biradical,[64] namely nucleophile addition to a dialdehyde intermediate, Friedel−Crafts alkylation and finally oxidation using 2,3-dichloro-5,6-dicyanobenzoquinone (DDQ, Scheme 3). Suzuki cross-coupling of either 2-naphthaleneboronic acid with dibromide **23**[65] or 1,4-phenylenediboronic acid with bromide **24**[63,66] gave dialdehydes **25** and **26**, respectively, in excellent yield. Treatment of these with

DOI: 10.1021/jacs.6b11397
J. Am. Chem. Soc. 2016, 138, 16827−16838

Scheme 3. Synthesis of DNI 7b and DPI 10b

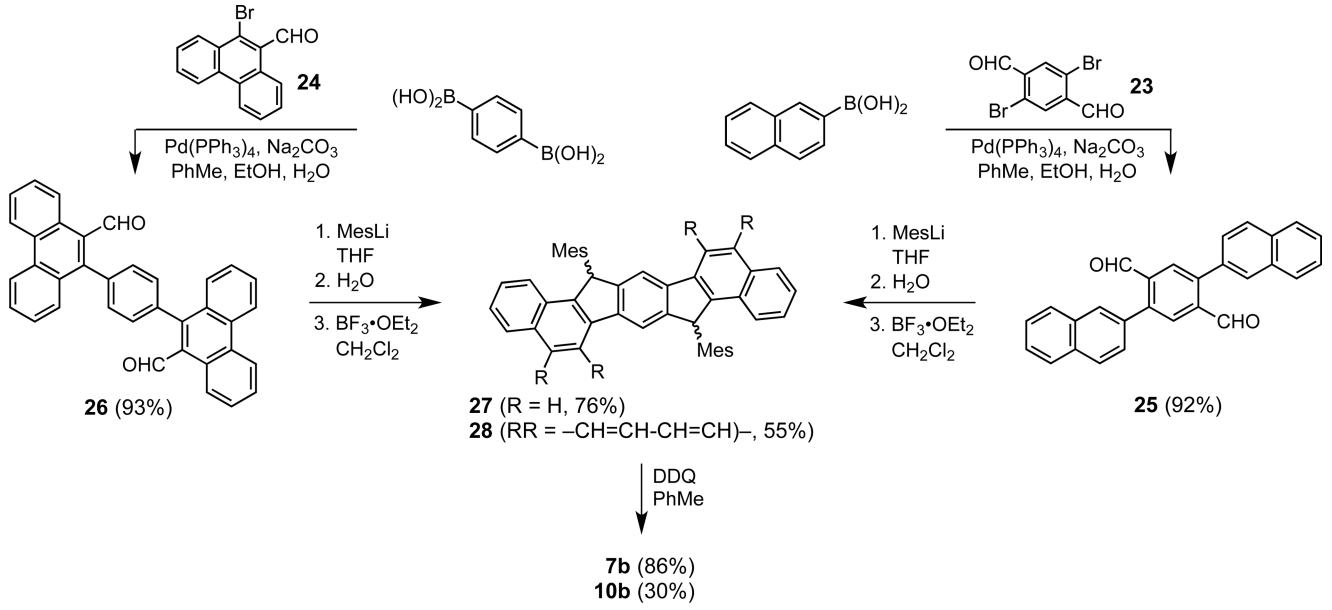

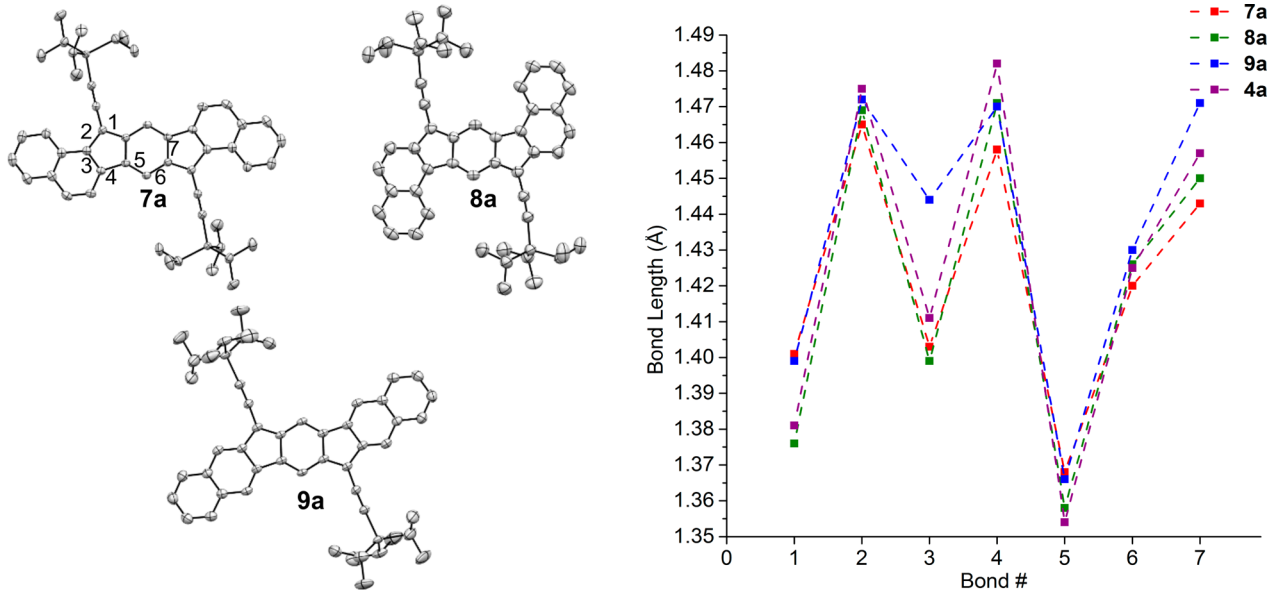

Figure 3. (left) Molecular structures of DNIs **7a**–**9a**; hydrogen atoms emitted for clarity; ellipsoids are set to 50% probability. (right) Comparison of the bond alternation in the indacene core of the three DNI isomers with indeno[1,2-*b*]fluorene **4a**; bond numbering is shown in the structure of **7a**.

mesityllithium followed by cyclization of the crude diols using $BF_3{\cdot}OEt_2$ afforded the dihydro intermediates **27** and **28**. Subsequent oxidation using DDQ furnished dark blue indacenes **7b** and **10b** in moderate to good yield.

Solid-State Structures. Single crystals of **7a**–**9a** suitable for X-ray diffraction were grown via slow diffusion of MeCN into $CDCl_3$ at −40 °C. DNIs **7a**–**9a** (Figure 3, left) each show a planar, *p*-xylylene-like structure in the solid state with pronounced bond length alternation within the indacene core. The fused bond between the naphthalene and indacene moieties, bond 3, exhibits significant variation between the DNI isomers (Figure 3, right). In the *anti*-(**7a**) and *syn*-DNIs (**8a**), bond 3 has a length of 1.401 and 1.403 Å, respectively, whereas in the *linear*-DNI (**9a**), bond 3 has lengthened to 1.440 Å. For comparison, bond 3 in the X-ray structure of *syn*-DNI **8b** is similarly short (1.401 Å; see Supporting Information). This variation is not unexpected due to the bond length differences in naphthalene: the *anti*- and *syn*-DNIs have the indacene core fused to the 1,2-bond of the outer naphthalene moieties whereas the *linear*-DNI is fused to the 2,3-bond. The 1,2-bond in naphthalene is well-known to be significantly shorter than the 2,3-bond.[67] Similar variation was also observed in the X-ray structures of the dinaphthopentalene series.[47,57]

Electronic Properties. Figure 4 shows the electronic absorption spectra of **7**–**10** along with the spectra for **4**. Although the TIPS-ethynyl DNIs display a similar strong absorption near 350 nm, they have large differences in their low-energy absorptions, which are bathochromically shifted versus **4a** with λ_{max} values of 654 (*anti*-**7a**), 634 (*syn*-**8a**), and 595 nm (*linear*-**9a**). For comparison, λ_{max} values of DPI **10a** and [1,2-*b*]IF **4a** are 692 and 568 nm, respectively. DNIs **7a**–**9a** also exhibit molar absorptivity values 1.6–2.4 times higher

DOI: 10.1021/jacs.6b11397
J. Am. Chem. Soc. 2016, 138, 16827–16838

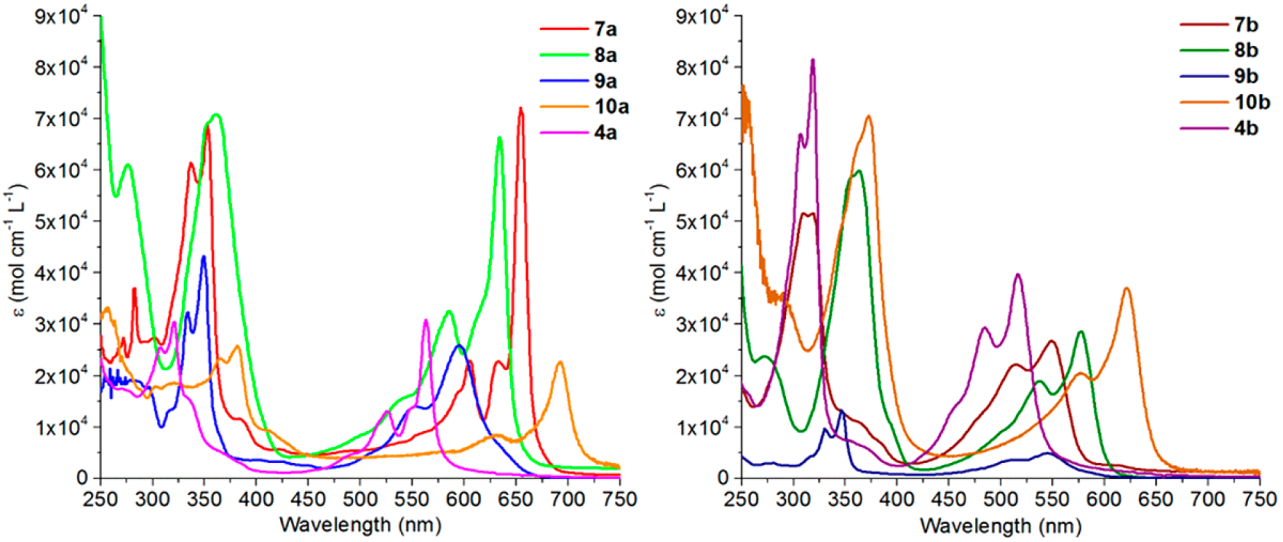

Figure 4. Electronic absorption spectra of the TIPS-ethynyl (**a**, left) and mesityl (**b**, right) derivatives of diareno-indacenes **7**−**10** and comparison with the [1,2-*b*]IF analogues **4a**,**b**.

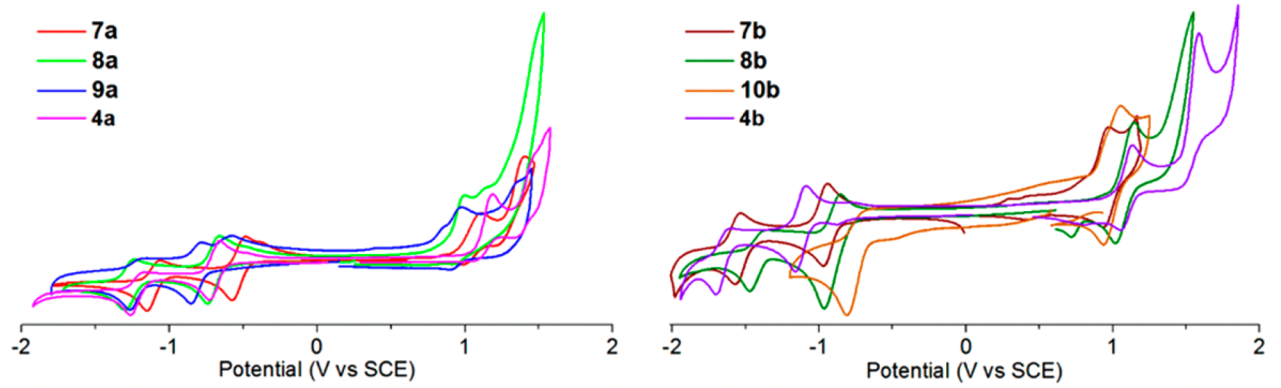

Figure 5. Cyclic voltammograms of the TIPS-ethynyl (**a**, left) and mesityl (**b**, right) derivatives of diarenoindacenes **7**−**10** and comparison with the [1,2-*b*]IF analogues **4a**,**b**.

Table 1. Electrochemical and Optical Data for DNIs 7-9, DPI 10 and [1,2-*b*]IF 4

	electrochemical[a]						optical[b]		
compound	E^1_{red} (V)	E^2_{red} (V)	E_{ox} (V)	LUMO (eV)	HOMO (eV)	E_{gap} (eV)	λ_{max} (nm)	λ_{onset} (nm)	E_{gap} (eV)
7a	−0.53	−1.11	1.04	−4.11	−5.68	1.57	654	667	1.86
8a	−0.70	−1.27	1.02	−3.95	−5.66	1.72	634	648	1.91
9a	−0.81	−1.21	0.94	−3.83	−5.58	1.75	595	633	1.95
10a	—	—	—	—	—	—	692	720	1.72
4a[c]	−0.69	−1.20	1.20	−4.00	−5.88	1.89	568	584	2.12
7b	−0.96	−1.55	0.95	−3.68	−5.59	1.91	549	577	2.15
8b	−0.92	−1.44	1.09	−3.72	−5.73	2.01	578	587	2.11
9b	—	—	—	—	—	—	543	560	2.21
10b	−0.77	—	1.09	−3.87	−5.73	1.86	622	629	1.97
4b[d]	−1.12	−1.73	1.10	−3.52	−5.74	2.22	516	541	2.29

[a]CVs were recorded on 1−5 mM of analyte in 0.1 M Bu_4NBF_4/CH_2Cl_2 at a scan rate of 50 mV s^{-1} with a glassy carbon working electrode, a Pt coil counter electrode, and a Ag wire pseudoreference. Values reported as the half-wave potential (vs SCE) using the Fc/Fc^+ couple (0.46 V in CH_2Cl_2) as an internal standard. HOMO and LUMO energy levels in eV were approximated using SCE = −4.64 eV vs vacuum and $E_{1/2}$ values for reversible processes or E_p values for irreversible processes. [b]Spectra were obtained in C_6H_{12} using stock solutions of the analyte in $CHCl_3$. The optical HOMO/LUMO energy gap/absorbance onset was determined as the intersection of the *x*-axis and a tangent line passing through the inflection point of the lowest energy absorption. [c]Reference 51. [d]Reference 50.

than that of **4a** at their respective λ_{max} values. Unlike the TIPS-ethynyl compounds, the mesityl derivatives **7b**−**10b** (with the exception of **9b**) show similar molar absorptivities to **4b**. Although the mesityl compounds also share a similar high-energy absorbance between 315 and 375 nm, their low-energy absorbances are less bathochromically shifted (549 (*anti*-**7b**),

DOI: 10.1021/jacs.6b11397
J. Am. Chem. Soc. 2016, 138, 16827−16838

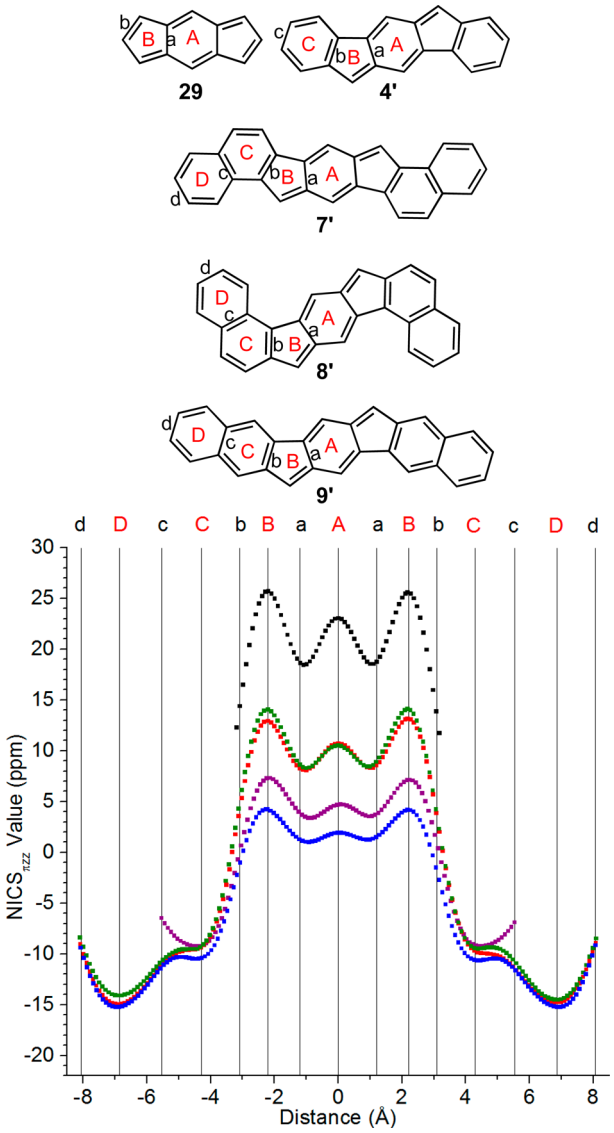

Figure 6. NICS-XY scans of *s*-indacene (**29**, black), **7′** (red), **8′** (green), [1,2-*b*]IF **4′** (purple), and **9′** (blue) listed in order of decreasing paratropicity of the indacene core.

578 (*syn*-**8b**), 543 (*linear*-**9b**), and 622 nm (DPI **10b**)) than in the corresponding TIPS-ethynyl derivatives. This 50−100 nm difference can be explained because of the loss of the conjugation with the alkynes combined with the fact that the mesityl groups are nearly orthogonal (>75° dihedral) to the indenofluorene backbone, thus limiting significant electronic communication.[50,59]

The redox behavior of **7**−**10** (with the exception of **9b** and **10a**, which could not be adequately analyzed due to low solubility) was examined by cyclic voltammetry (Figure 5); the compiled electrochemical and optical data for these compounds, along with the data for **4**, are given in Table 1. All three DNI isomers have one reversible reduction along with a second reduction of varying reversibility. The E^1_{red} values for the three TIPS-ethynyl DNIs straddle that of **4** (−0.69 V vs SCE):[51] the E^1_{red} for **8a** is −0.70 V, similar to the first reduction for **4a**, whereas the E^1_{red} for **7a** is nearly 200 mV less negative at −0.53 V, and E^1_{red} for **9a** is over 100 mV more negative at −0.82 V. All three ethynylated DNI isomers also show a quasi-reversible oxidation, with the potential values exhibiting a reversed trend to the reduction potentials. A*nti*-**7a** has the most positive oxidation potential at 1.04 V and *linear*-**9a** the least positive potential at 0.94 V. Unlike the reductions, however, all three DNI isomers oxidize at less positive potentials than that of **4a** (1.20 V). The mesityl DNIs **8b** and **9b** show similar E^1_{red} values at −0.96 and −0.92 V, respectively. Electrochemical analysis of the soluble mesityl DPI derivative **10b** gave a E^1_{red} value of −0.77 V, over 150 mV less negative than those of the two mesityl DNIs.

Computational Studies. The significant differences in the optoelectronic properties of the three DNI isomers spurred us to perform a detailed computational investigation of these and related diareno-fused antiaromatic compounds. The variability in the absorption spectra and reduction potentials of **7**−**9** suggested a possible difference in the antiaromatic character of the molecules. One factor in the electron accepting ability of indenofluorene derivatives is the fact that upon reduction, the antiaromatic character of the indacene core is eliminated and some degree of aromaticity is established;[50,51,68,69] thus, a less negative reduction potential may indicate that a compound possesses stronger paratropicity, similar to the related indacenodibenzothiophene (IDBT) scaffold produced by our lab. The IDBT molecules have highly positive NICS$_{\pi ZZ}$ values for their tricyclic cores, values nearly identical as those calculated for *s*-indacene, and show E^1_{red} potentials between −0.37 and −0.46 V for the TIPS-ethynyl derivatives.[58,59]

To explore the ring currents in DNIs **7**−**9**, we utilized two newly developed nucleus independent chemical shift (NICS) methodologies, the NICS-XY scan and π-only methods.[70−72] NICS-XY scans are important for the DNI systems because of the presence of both paratropic and diatropic ring currents in such large polycyclic molecules containing both (4*n*) and (4*n* +2) π-electron circuits. Examining a single point above the center of each ring (as in traditional NICS(1) calculations) may not produce an accurate depiction of the electronic currents in these molecules. The NICS-XY scan allows us to explore local, semiglobal and global ring currents as well as the type of current(s) (e.g., diatropic vs paratropic) within a particular molecular skeleton. The π-only model removes the contribution of the σ-electrons from the NICS values, affording data produced solely from π-electron ring currents. Comparison of the NICS$_{ZZ}$ and the NICS$_{\pi ZZ}$ results for all calculated indacene structures is given in Figures S1−S3 in the Supporting Information. All NICS-XY scans were performed with the RB3LYP functional. To validate this practice, select compounds were also calculated with the UB3LYP functional, and both methods produce NICS values that are essentially identical (Figure S4). To limit calculation time and simplify comparisons, all computations were performed on the parent compounds with no substitution on the five-membered rings. Comparison between the diethynyl and parent DNIs (Figure S5) indicates the largest differences in NICS$_{\pi ZZ}$ values are less than 2 ppm, confirming the validity of this "simplified" approach.

To set a baseline for antiaromaticity, the NICS-XY scan of *s*-indacene (**29**) was first calculated (Figure 6, black).[73] Compound **29** shows a global paratropic current and peak local currents above each ring, with NICS$_{\pi ZZ}$ values of 18 ppm over bond a, and a maximum NICS$_{\pi ZZ}$ value of 25.4 ppm over ring B. Comparing the NICS-XY scan of *s*-indacene with that of "simplified" [1,2-*b*]IF **4′** illuminates the effect of benzo fusion on the antiaromaticity of the indacene core (Figure 6, purple). Compound **4′** shows less intense paratropic ring currents over

DOI: 10.1021/jacs.6b11397
J. Am. Chem. Soc. 2016, 138, 16827−16838

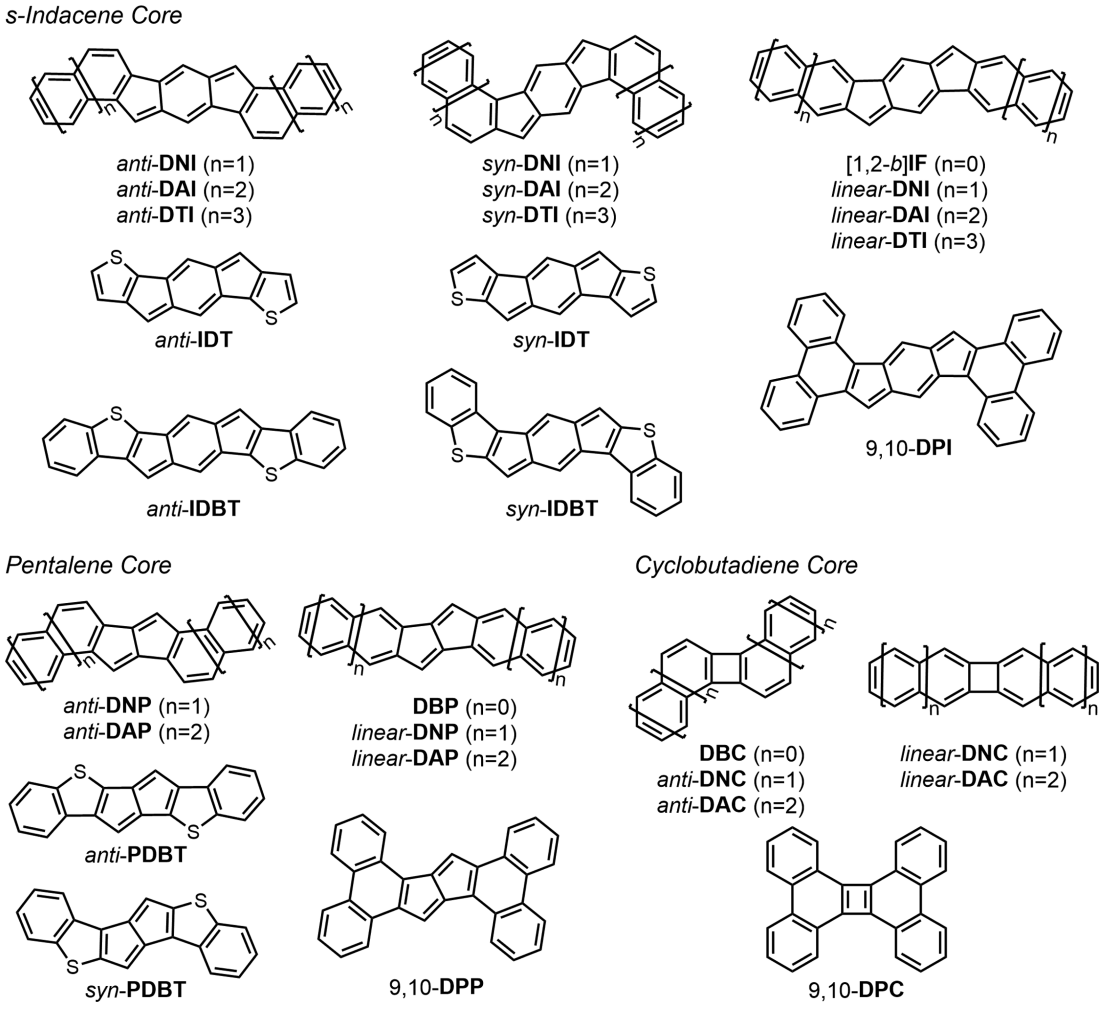

Figure 7. Structures used for the NICS-XY scan calculations. Parent structures were used to simplify comparisons and reduce computational time.

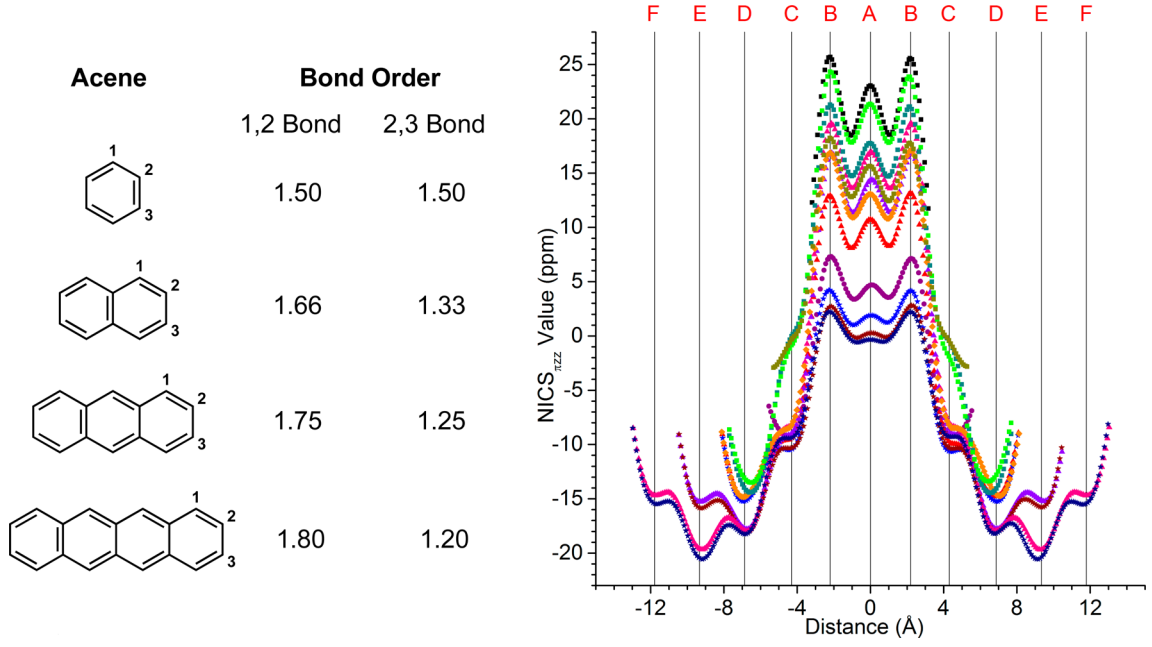

Figure 8. Bond orders of the fused bonds for the diarenoindacene proposed structures (left) and NICS-XY scans (right) of **29** (black ■), *syn*-**IDBT** (green ■), *anti*-**IDBT** (teal ■), *anti*-**DTI** (magenta ▲), *anti*-**IDT** (olive ■), 9,10-**DPI** (orange ◆), *anti*-**DAI** (purple ▲), **7′** (red ▲), **4′** (purple ●), **9′** (blue ★), *linear*-**DAI** (brown ★), and *linear*-**DTI** (navy ★) listed in order of decreasing paratropicity of the indacene core.

DOI: 10.1021/jacs.6b11397
J. Am. Chem. Soc. 2016, 138, 16827−16838

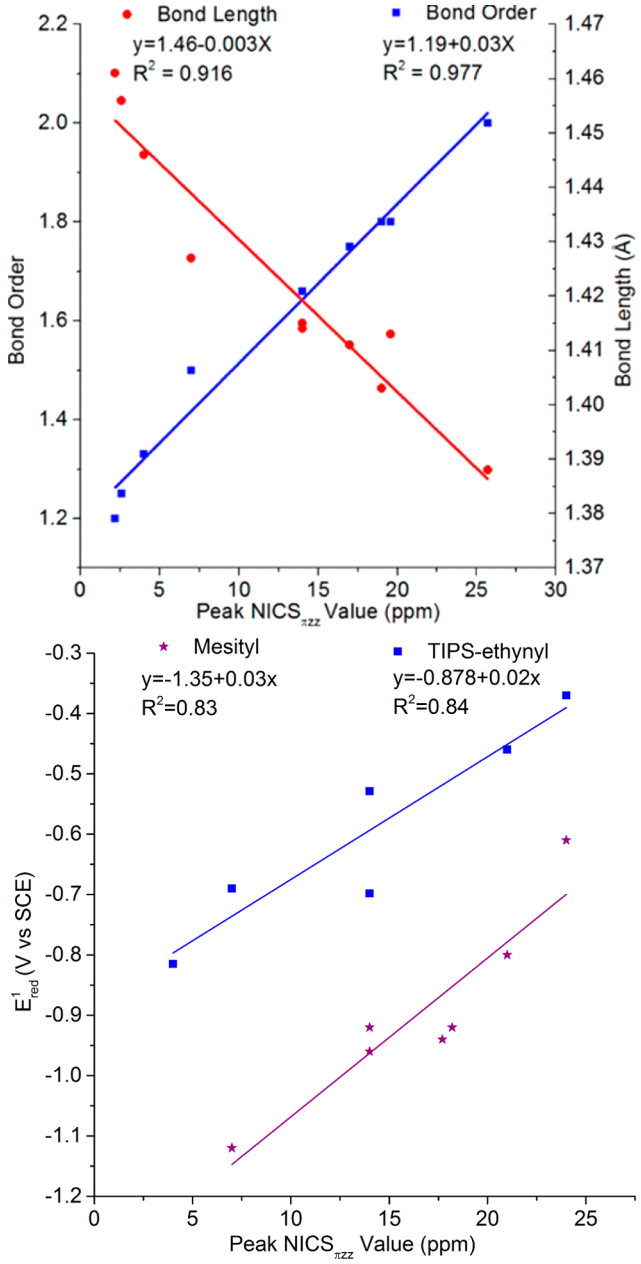

Figure 9. (top) Linear correlation between the peak NICS value in the core of a diarenoindacene and the bond order and bond length of the fusion bond. (bottom) Relation between peak NICS value and the measured E^1_{red} of mesityl- and TIPS-ethynyl-substituted compounds prepared in our lab.

the indacene core (3.4 and 7 ppm for the bond a and ring B values, respectively) than **29**, but the scan retains the same shape, with a semiglobal paratropic current over the indacene moiety and local peak currents over each ring. Fused to the indacene core of **4′** are aromatic benzene rings, which retain a substantial degree of diatropicity (NICS$_{\pi ZZ}$ values of −9 vs −17 ppm for benzene).[70]

Examination of the simplified DNI regioisomers reveals a striking difference in the NICS-XY scans depending upon how the naphthalene is fused to the indacene (Figure 6). Compounds **7′** (red trace) and **8′** (green trace), with the indacene core fused to the 1,2-bond of naphthalene, display very similar values (both 8 ppm over bond a and 13 and 14 ppm over ring B, respectively) with increased paratropic currents in the indacene core compared to IF **4′**. The *linear*-DNI **9′** (blue), however, has NICS$_{\pi ZZ}$ values for the indacene core lower than those of **4′**, peaking at 4 ppm over ring B and 1 ppm over bond a. Interestingly, whereas the peak NICS$_{\pi ZZ}$ values for the indacene core vary between 4.2 and 14.0 ppm for the DNI isomers, the range of values for the fused naphthalenes is very small, from −9 to −11 ppm for ring C and −14 to −15 ppm for ring D. The value for ring C in **4′** (−9.4 ppm) is well-bracketed by the DNI ring C values above.

Examination of the structures and the NICS$_{\pi ZZ}$ values of the core reveals a correlation between the double bond character of the fused bond and core paratropicity. In **7′** and **8′**, the two DNI isomers with higher NICS$_{\pi ZZ}$ values, the naphthalenes are fused to indacene via the 1,2-bond of the naphthalene moiety, which has a bond order of 1.66. The compound with core NICS$_{\pi ZZ}$ values in the closest proximity is **4′**, which has both lower NICS$_{\pi ZZ}$ values and a lower bond order of 1.5. In comparison, **9′**, which is fused to the 2,3-bond of naphthalene, has both the lowest bond order of 1.33 and the lowest NICS$_{\pi ZZ}$ values of the five compounds in Figure 6.

To confirm our hypothesis that fusion bond order drives core paratropicity, NICS-XY scans were performed on a series of structures (Figure 7) including unknown dianthracenoindacenes (DAI) and ditetracenoindacenes (DTI), as well as the 9,10-isomer of diphenanthrenoindacene (DPI). For completeness, these values were also compared with the NICS-XY scans for the previously reported indacenodithiophenes (IDTs) and indacenodibenzothiophenes (IDBTs).[58,59] All the computed compounds had similar planar structures to those of the DNIs. Similar to the results for the DNI isomers, the NICS values of the *syn* and *anti* isomers of the DAIs, DTIs, and IDTs are nearly identical; therefore, to make the data clearer, only the values of the *anti*-diareno isomers are plotted (see Figure S6 for the enlarged, complete data set).

Figure 8 shows that the DAIs and DTIs all follow the same trend as the DNIs, with the 1,2-fused isomers possessing more positive NICS$_{\pi ZZ}$ values for the indacene core than the 2,3-fused isomers. As the bond order of the 1,2-bond approaches 2 from DNI to DAI and finally DTI, the NICS$_{\pi ZZ}$ value over ring B in the core increases from 14 to 17 to 20 ppm, respectively. Similarly, the *linear*-DAI and -DTI have NICS$_{\pi ZZ}$ values over ring B that approach 0 as the bond order of the 2,3-bond becomes closer to 1. With the largest difference in bond order between the 1,2- and 2,3-bonds, the tetracene-fused DTIs exhibit the most significant difference in NICS$_{\pi ZZ}$ values: the *syn*-DTI shows a peak NICS$_{\pi ZZ}$ value of 20 ppm over ring B and a NICS$_{\pi ZZ}$ value of 14 ppm over bond a, whereas the *linear*-DTI has NICS$_{\pi ZZ}$ values of 2 and 0 ppm over ring B and bond a, respectively. Despite these large differences in core paratropicity, very little change in the diatropicity of the fused arenes is observed. Ring C values range from −8 to −11 ppm, and the other arene rings are even more diatropic (<−15 ppm). Using the DTIs for example again, while there is a 18 ppm difference in the NICS values above the indacene core, the largest variance in NICS values above the tetracene moieties is only 1.6 ppm. A similar lack of significant variation in the diatropicity of the outer rings is seen for the other diarenoindacene derivatives.

Comparison of the heteroatom-containing IDTs and IDBTs with the purely hydrocarbon compounds also supports the correlation between the double bond character of the fused bond and the NICS$_{\pi ZZ}$ value of the indacene core (Figure 8). *Anti*-IDT has a peak NICS value of 18 ppm, similar to the *anti*-

DOI: 10.1021/jacs.6b11397
J. Am. Chem. Soc. 2016, 138, 16827−16838

Table 2. Summary of Computational Data for All Compounds Examined

compound	NICS$_{\pi ZZ}$ values (ppm) core maximum[a]	core minimum[b]	1st fused arene[c]	fused bond length (Å)	HOMO (eV)	LUMO (eV)	E_{gap} (eV)
indacenes							
IF	7	1	−9	1.427	−5.47	−3.00	2.48
anti-DNI	14	8	−10	1.414	−5.37	−3.20	2.17
syn-DNI	14	8	−10	1.415	−5.37	−3.20	2.18
linear-DNI	4	3	−10	1.446	−5.16	−2.90	2.26
anti-DAI	17	11	−9	1.411	−5.13	−3.31	1.81
syn-DAI	19	12	−9	1.411	−5.10	−3.33	1.77
linear-DAI	2	0	−10	1.456	−4.92	−2.86	2.05
anti-DTI	20	14	−8	1.413	−4.91	−3.39	1.52
syn-DTI	22	15	−9	1.412	−4.90	−3.43	1.42
linear-DTI	1	−1	−9	1.461	−4.73	−2.86	1.87
9,10-DPI	17	11	−9	1.403	−5.30	−3.31	1.99
syn-IDT	17	12	−1	1.404	−5.35	−3.19	2.15
anti-IDT	18	13	0	1.401	−5.30	−3.14	2.16
syn-IDBT	24	18	0	1.397	−5.24	−3.42	1.82
anti-IDBT	21	15	0	1.407	−5.25	−3.30	1.94
pentalenes							
DBP	12	8	−8	1.430	−5.70	−2.62	3.08
anti-DNP	20	16	−9	1.411	−5.27	−2.89	2.38
linear-DNP	7	4	−9	1.452	−5.51	−2.50	3.01
anti-DAP	25	21	−10	1.404	−4.98	−3.05	1.93
linear-DAP	4	2	−9	1.463	−5.13	−2.44	2.69
9,10-DPP	25	20	−10	1.392	−5.15	−3.03	2.12
syn-PDBT	34	29	−1	1.382	−5.10	−3.06	2.04
anti-PDBT	33	28	−1	1.387	−5.09	−3.07	2.02
cyclobutadienes							
biphenylene	8	N/A	−7	1.424	−5.66	−1.60	4.06
syn-DNC	17	N/A	−9	1.403	−5.06	−2.22	2.84
linear-DNC	4	N/A	−8	1.446	−5.85	−1.95	3.90
syn-DAC	22	N/A	−10	1.394	−4.73	−2.61	2.12
linear-DAC	2	N/A	−9	1.456	−5.40	−2.44	2.96
9,10-DPC	21	N/A	−11	1.381	−4.87	−2.42	2.45

[a]The maximum NICS$_{\pi ZZ}$ value in the paratropic core. This is above one of the five membered rings in the indacene- and pentalene-based compounds and above the four membered rings in the cyclobutadiene-based compounds. [b]The minimum NICS$_{\pi ZZ}$ value in the paratropic core. This is above the bond between the five- and six-membered rings in the indacene system and above the center bond in the pentalene system. There is no minimum in the cyclobutadiene system due to it showing a single peak. [c]NICS value over the center of the aromatic ring fused directly to the antiaromatic core.

DAI. This can be explained by the lower aromaticity of the thiophene ring, which allows the thiophene 1,2-bond to retain more double bond character than that of a CC bond in benzene or naphthalene. The IDBT isomers show even more positive NICS$_{\pi ZZ}$ values, with peak *syn* and *anti* values of 24 and 21 ppm, respectively, over ring B, values nearly as large as that of *s*-indacene itself (25 ppm). Previous studies on these compounds revealed that benzo fusion to the outer thiophene rings extinguishes the weak ring current of the thiophene portion, which instead acts as a spacer between the strongly diatropic outer benzene ring and the highly paratropic indacene core. Thus, the large NICS$_{\pi ZZ}$ values observed in the indacene unit of the IDBTs are fueled by the high double bond character of the indacene-benzothiophene fusion.[59]

To visualize better the relationship between the double bond character of the fused arene bond and the NICS$_{\pi ZZ}$ value of the indacene core, the bond order and the bond length of the fusion bond were plotted versus the maximum NICS$_{\pi ZZ}$ value in the core (Figure 9, top). There is a clear relationship between the double bond character of the fusion bond and the NICS$_{\pi ZZ}$ value in the indacene core, with more double-bond-like, shorter bonds leading to more intense paratropic ring currents. To relate the calculated NICS$_{\pi ZZ}$ values to a measurable parameter, a plot of the peak NICS$_{\pi ZZ}$ value versus the E^1_{red}, using the available data for the TIPS-ethynyl- and mesityl-substituted compounds (Figure 9, bottom),[50,51,59] depicts a trend of higher NICS$_{\pi ZZ}$ values correlating to less negative reduction potentials. This follows the hypothesis that part of the electron-accepting ability of indenofluorene, and diarenoindacene compounds in general, is a result of removing the destabilization of the antiaromatic core; therefore, compounds with greater paratropicity are more easily reduced, which in turn imparts diatropic character.[68,69]

With this relationship apparent for diarenoindacene compounds, we decided to investigate if this trend could be applied to other diareno-antiaromatic compounds. NICS-XY scans were performed on a series of diarenopentalenes and diarenocyclobutadienes (Figure 7), and a summary of the computational data for the three sets of compounds is presented in Table 2. Diarenopentalenes were chosen because they have received significant investigation in recent years as promising organic semiconductors.[36,46,47,54] In addition to

DOI: 10.1021/jacs.6b11397
J. Am. Chem. Soc. 2016, 138, 16827−16838

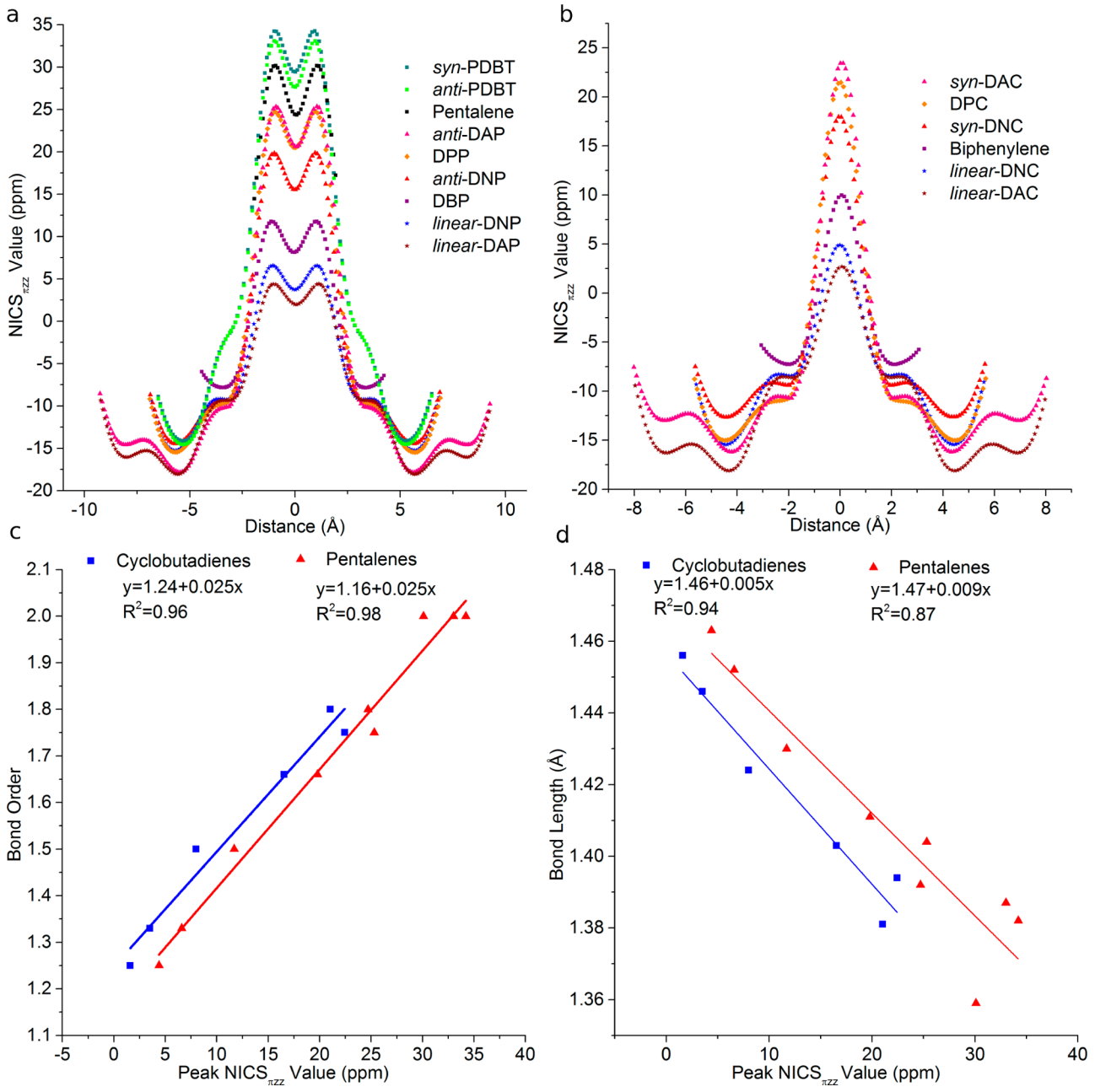

Figure 10. (a) NICS-XY scans of diarenopentalenes, (b) NICS-XY scans of diarenocyclobutadienes, (c) bond order vs NICS$_{\pi ZZ}$ values, and (d) bond length vs NICS$_{\pi ZZ}$ values. Compounds in graphs a and b are listed in order of decreasing paratropicity of the indacene core.

materials applications,[74,75] diarenocyclobutadienes are derivatives of biphenylene, which has long been of interest to organic chemists as a stable example of a cyclobutadiene ring.[19,76−78] The NICS-XY plots of both the pentalene and cyclobutadiene series show a similar shape to those of the diarenoindacenes, with peak positive NICS$_{\pi ZZ}$ values over the core and outer rings that have similar negative NICS$_{\pi ZZ}$ values to those of the diarenoindacenes (Figure 10a,b). When the peak NICS$_{\pi ZZ}$ values are plotted against the double bond character of the fusion bond and its bond length, the results again show that shorter, more double-bond-like fused bonds lead to higher NICS$_{\pi ZZ}$ values in the core (Figure 10c,d). Because many diarenopentalene derivatives have been reported in the literature along with their corresponding reduction potentials,[46−48,54] their calculated NICS$_{\pi ZZ}$ values can be plotted against their E^1_{red} potential (Figure S7). This reveals the same trend as in the diarenoindacenes (Figure 9, bottom), where compounds that display more intense paratropic currents in the core also show less negative reduction potentials.

Experimental Evaluation. To confirm the predictive power of these computations, we prepared the diphenanthrenoindacene (DPI) isomer **10** with the indacene core fused to the 9,10-bond of phenanthrene, as this bond is well-known to possess significant double bond character (bond order of 1.8). Its high NICS$_{\pi ZZ}$ value for the indacene B ring (17 ppm) is well-bracketed by the *syn*/*anti*-DAI and -DTI isomers, yet 9,10-DPIs **10** are synthetically more accessible as shown in Schemes 2 and 3. Although **10a** was not soluble enough to perform accurate cyclic voltammetry, CV data for **10b** (Figure 5, bottom) exhibit a E^1_{red} of −0.77 mV, significantly less negative

DOI: 10.1021/jacs.6b11397
J. Am. Chem. Soc. 2016, 138, 16827−16838

than those of the mesityl compounds with lower peak NICS values. Thus, this value further corroborates the general trend described above (see Figure S8).

CONCLUSIONS

We have disclosed the synthesis of three new symmetric dinaphthoindacene isomers **7**–**9** along with a 9,10-fused diphenanthrenoindacene analogue **10**, substituted with either (triisopropylsilyl)ethynyl (**a**) or mesityl (**b**) groups, and have examined their electronic structure by absorption spectroscopy and cyclic voltammetry. Computational investigations revealed that the intensity of the paratropic currents in the antiaromatic core of diarenoindacene derivatives can be controlled by varying the double bond character of the fused bond between the outer arene groups and the indacene core, a trend also observed in other diareno-fused antiaromatic compounds such as diarenopentalenes and diarenocyclobutadienes. In the design of new materials for use in organic semiconductor applications, especially with the desire to tune the balance of aromaticity and antiaromaticity in a compound, close attention must be paid to the bond order of the fusion bond. Decisions on which isomer to prepare made solely on the ease of synthesis may inadvertently give products with significantly different properties than those desired. The ability to control antiaromaticity with only small changes in structure will also allow further exploration of the relationship of related properties like diradical character.[64,79,80]

Estimated by NICS-XY scan calculations, the intensity of the paratropic ring current in the internal core of all three classes of antiaromatic molecules can be varied substantially without significant change in the diatropic ring currents in the fused aromatic rings. This work demonstrates that seemingly trivial differences in the structure of fused diarenoantiaromatics can lead to drastic differences in both their optical and electronic properties, the latter of which was shown by a linear correlation when plotting the calculated $NICS_{\pi ZZ}$ values against the known E^1_{red} potentials, i.e., the greater the degree of antiaromaticity, the easier it is to reduce the molecule, thus leading to aromatic stabilization. Future work on the diarenoindacenes will examine the preparation of even longer fused arenes as well as manipulation of molecular packing in the solid state.

ASSOCIATED CONTENT

Supporting Information

The Supporting Information is available free of charge on the ACS Publications website at DOI: 10.1021/jacs.6b11397.

Experimental procedures, computational details and *xyz* coordinates, and copies of spectra (PDF)
Crystallographic data for **7a** (CIF)
Crystallographic data for **8a** (CIF)
Crystallographic data for **8b** (CIF)
Crystallographic data for **9a** (CIF)

AUTHOR INFORMATION

Corresponding Author

*haley@uoregon.edu

ORCID

Michael M. Haley: 0000-0002-7027-4141

Notes

The authors declare no competing financial interest.

ACKNOWLEDGMENTS

We thank the National Science Foundation (CHE-1301485 and CHE-1565780) for support of the research, as well as support in the form of an instrumentation grant (CHE-1427987). HRMS were obtained at the Biomolecular Mass Spectrometry Core of the Environmental Health Sciences Core Center at Oregon State University (NIH P30ES000210).

REFERENCES

(1) Krygowski, T. M.; Cyranski, M. K.; Czarnocki, Z.; Hafelinger, G.; Katritzky, A. R. *Tetrahedron* **2000**, *56*, 1783–1796.
(2) Clar, E.; Macpherson, I. A. *Tetrahedron* **1962**, *18*, 1411–1416.
(3) Armit, J.; Robinson, R. *J. Chem. Soc., Trans.* **1925**, *127*, 1604–1617.
(4) Kekule, A. *Bull. Soc. Chim. Fr.* **1885**, *3*, 98.
(5) Hückel, E. *Eur. Phys. J. A* **1931**, *70*, 204–286.
(6) Willstätter, R.; Waser, E. *Ber. Dtsch. Chem. Ges.* **1911**, *44*, 3423–3445.
(7) Ladenburg, A. *Justus Liebigs Ann. Chem.* **1874**, *172*, 331–356.
(8) Heidelberg, E. E. *Justus Liebigs Ann. Chem.* **1866**, *137*, 327–359.
(9) Wiberg, K. B. *Chem. Rev.* **2001**, *101*, 1317–1331.
(10) Breslow, R.; Brown, J.; Gajewski, J. *J. Am. Chem. Soc.* **1967**, *89*, 4383–4390.
(11) Breslow, R. *Acc. Chem. Res.* **1973**, *6*, 393–398.
(12) Nishinaga, T.; Ohmae, T.; Iyoda, M. *Symmetry* **2010**, *2*, 76–97.
(13) Sung, Y. M.; Oh, J.; Kim, W.; Mori, H.; Osuka, A.; Kim, D. *J. Am. Chem. Soc.* **2015**, *137*, 11856–11859.
(14) Jartín, R. S.; Ligabue, A.; Soncini, A.; Lazzeretti, P. *J. Phys. Chem. A* **2002**, *106*, 11806–11814.
(15) Nishinaga, T.; Ohmae, T.; Aita, K.; Takase, M.; Iyoda, M.; Arai, T.; Kunugi, Y. *Chem. Commun.* **2013**, *49*, 5354–5356.
(16) Allen, A. D.; Tidwell, T. T. *Chem. Rev.* **2001**, *101*, 1333–1348.
(17) Sugawara, S.; Hirata, Y.; Kojima, S.; Yamamoto, Y.; Miyazaki, E.; Takimiya, K.; Matsukawa, S.; Hashizume, D.; Mack, J.; Kobayashi, N.; Fu, Z.; Kadish, K. M.; Sung, Y. M.; Kim, K. S.; Kim, D. *Chem. - Eur. J.* **2012**, *18*, 3566–3581.
(18) Bally, T.; Chai, S.; Neuenschwander, M.; Zhu, Z. *J. Am. Chem. Soc.* **1997**, *119*, 1869–1875.
(19) Breslow, R.; Schneebeli, S. T. *Tetrahedron* **2011**, *67*, 10171–10178.
(20) Cao, J.; London, G.; Dumele, O.; von Wantoch Rekowski, M.; Trapp, N.; Ruhlmann, L.; Boudon, C.; Stanger, A.; Diederich, F. *J. Am. Chem. Soc.* **2015**, *137*, 7178–7188.
(21) Breslow, R.; Foss, F. W., Jr *J. Phys.: Condens. Matter* **2008**, *20*, 374104.
(22) Mei, J.; Diao, Y.; Appleton, A. L.; Fang, L.; Bao, Z. *J. Am. Chem. Soc.* **2013**, *135*, 6724–6746.
(23) Bendikov, M.; Wudl, F.; Perepichka, D. F. *Chem. Rev.* **2004**, *104*, 4891–4946.
(24) Anthony, J. E.; Facchetti, A.; Heeney, M.; Marder, S. R.; Zhan, X. *Adv. Mater.* **2010**, *22*, 3876–3892.
(25) Schlenker, C. W.; Thompson, M. E. *Top. Curr. Chem.* **2011**, *312*, 175–212.
(26) Ahmed, E.; Ren, G.; Kim, F. S.; Hollenbeck, E. C.; Jenekhe, S. A. *Chem. Mater.* **2011**, *23*, 4563–4577.
(27) Eftaiha, A. F.; Sun, J.-P.; Hill, I. G.; Welch, G. C. *J. Mater. Chem. A* **2014**, *2*, 1201–1213.
(28) Wu, J.; Pisula, W.; Müllen, K. *Chem. Rev.* **2007**, *107*, 718–747.
(29) Giri, G.; Verploegen, E.; Mannsfeld, S. C.; Atahan-Evrenk, S.; Kim do, H.; Lee, S. Y.; Becerril, H. A.; Aspuru-Guzik, A.; Toney, M. F.; Bao, Z. *Nature* **2011**, *480*, 504–508.
(30) Anthony, J. E.; Brooks, J. S.; Eaton, D. L.; Parkin, S. R. *J. Am. Chem. Soc.* **2001**, *123*, 9482–9483.
(31) Payne, M. M.; Parkin, S. R.; Anthony, J. E. *J. Am. Chem. Soc.* **2005**, *127*, 8028–8029.
(32) Fudickar, W.; Linker, T. *J. Am. Chem. Soc.* **2012**, *134*, 15071–15082.
(33) Anthony, J. E. *Angew. Chem., Int. Ed.* **2008**, *47*, 452–483.

DOI: 10.1021/jacs.6b11397
J. Am. Chem. Soc. 2016, 138, 16827–16838

(34) Zade, S. S.; Zamoshchik, N.; Reddy, A. R.; Fridman-Marueli, G.; Sheberla, D.; Bendikov, M. *J. Am. Chem. Soc.* **2011**, *133*, 10803−10816.
(35) Schleyer, P. v. R.; Manoharan, M.; Jiao, H.; Stahl, F. *Org. Lett.* **2001**, *3*, 3643−3646.
(36) Mei, J.; Diao, Y.; Appleton, A. L.; Fang, L.; Bao, Z. *J. Am. Chem. Soc.* **2013**, *135*, 6724−6746.
(37) Cao, J.; London, G.; Dumele, O.; von Wantoch Rekowski, M.; Trapp, N.; Ruhlmann, L.; Boudon, C.; Stanger, A.; Diederich, F. *J. Am. Chem. Soc.* **2015**, *137*, 7178−7188.
(38) Zhang, L.; Fonari, A.; Liu, Y.; Hoyt, A. M.; Lee, H.; Granger, D.; Parkin, S.; Russell, T. P.; Anthony, J. E.; Bredas, J.-L.; Coropceanu, V.; Briseno, A. L. *J. Am. Chem. Soc.* **2014**, *136*, 9248−9251.
(39) Bhosale, S. V.; Jani, C. H.; Langford, S. J. *Chem. Soc. Rev.* **2008**, *37*, 331−342.
(40) Jiang, W.; Xiao, C.; Hao, L.; Wang, Z.; Ceymann, H.; Lambert, C.; Di Motta, S.; Negri, F. *Chem. - Eur. J.* **2012**, *18*, 6764−6775.
(41) Mamada, M.; Katagiri, H.; Mizukami, M.; Honda, K.; Minamiki, T.; Teraoka, R.; Uemura, T.; Tokito, S. *ACS Appl. Mater. Interfaces* **2013**, *5*, 9670−9677.
(42) Kim, C.; Huang, P. Y.; Jhuang, J. W.; Chen, M. C.; Ho, J. C.; Hu, T. S.; Yan, J. Y.; Chen, L. H.; Lee, G. H.; Facchetti, A.; Marks, T. J. *Org. Electron.* **2010**, *11*, 1363−1375.
(43) Vande Velde, C. M. L.; Balandier, J.; Stas, S.; Sergeyev, S.; Geerts, Y. H.; Tylleman, B. *Org. Lett.* **2011**, *13*, 5208−5211.
(44) Yamamoto, T.; Shinamura, S.; Miyazaki, E.; Takimiya, K. *Bull. Chem. Soc. Jpn.* **2010**, *83*, 120−130.
(45) Niimi, K.; Kang, M. J.; Miyazaki, E.; Osaka, I.; Takimiya, K. *Org. Lett.* **2011**, *13*, 3430−3433.
(46) Shen, J.; Yuan, D.; Qiao, Y.; Shen, X.; Zhang, Z.; Zhong, Y.; Yi, Y.; Zhu, X. *Org. Lett.* **2014**, *16*, 4924−4927.
(47) Kawase, T.; Fujiwara, T.; Kitamura, C.; Konishi, A.; Hirao, Y.; Matsumoto, K.; Kurata, H.; Kubo, T.; Shinamura, S.; Mori, H.; Miyazaki, E.; Takimiya, K. *Angew. Chem., Int. Ed.* **2010**, *49*, 7728−7732.
(48) Dai, G.; Chang, J.; Shi, X.; Zhang, W.; Zheng, B.; Huang, K. W.; Chi, C. *Chem. - Eur. J.* **2015**, *21*, 2019−2028.
(49) Chase, D. T.; Rose, B. D.; McClintock, S. P.; Zakharov, L. N.; Haley, M. M. *Angew. Chem., Int. Ed.* **2011**, *50*, 1127−1130.
(50) Chase, D. T.; Fix, A. G.; Kang, S. J.; Rose, B. D.; Weber, C. D.; Zhong, Y.; Zakharov, L. N.; Lonergan, M. C.; Nuckolls, C.; Haley, M. M. *J. Am. Chem. Soc.* **2012**, *134*, 10349−10352.
(51) Chase, D. T.; Fix, A. G.; Rose, B. D.; Weber, C. D.; Nobusue, S.; Stockwell, C. E.; Zakharov, L. N.; Lonergan, M. C.; Haley, M. M. *Angew. Chem., Int. Ed.* **2011**, *50*, 11103−11106.
(52) Chen, W.; Li, H.; Widawsky, J. R.; Appayee, C.; Venkataraman, L.; Breslow, R. *J. Am. Chem. Soc.* **2014**, *136*, 918−920.
(53) Mahendran, A.; Gopinath, P.; Breslow, R. *Tetrahedron Lett.* **2015**, *56*, 4833−4835.
(54) Konishi, A.; Fujiwara, T.; Ogawa, N.; Hirao, Y.; Matsumoto, K.; Kurata, H.; Kubo, T.; Kitamura, C.; Kawase, T. *Chem. Lett.* **2010**, *39*, 300−301.
(55) Dai, G.; Chang, J.; Zhang, W.; Bai, S.; Huang, K.; Xu, J.; Chi, C. *Chem. Commun.* **2015**, *51*, 503−506.
(56) Zheng, J.; Zhuang, X.; Qiu, L.; Xie, Y.; Wan, X.; Lan, Z. *J. Phys. Chem. A* **2015**, *119*, 3762−3769.
(57) Kato, S.; Kuwako, S.; Takahashi, N.; Kijima, T.; Nakamura, Y. *J. Org. Chem.* **2016**, *81*, 7700−7710.
(58) Young, B. S.; Chase, D. T.; Marshall, J. L.; Vonnegut, C. L.; Zakharov, L. N.; Haley, M. M. *Chem. Sci.* **2014**, *5*, 1008−1014.
(59) Marshall, J. L.; Uchida, K.; Frederickson, C. K.; Schütt, C.; Zeidell, A. M.; Goetz, K. P.; Finn, T. W.; Jarolimek, K.; Zakharov, L. N.; Risko, C.; Herges, R.; Jurchescu, O. D.; Haley, M. M. *Chem. Sci.* **2016**, *7*, 5547−5558.
(60) Ota, S.; Minami, S.; Hirano, K.; Satoh, T.; Ie, Y.; Seki, S.; Aso, Y.; Miura, M. *RSC Adv.* **2013**, *3*, 12356−12365.
(61) Lee, I. H.; Gong, M. S. *Bull. Korean Chem. Soc.* **2011**, *32*, 1475−1482.
(62) Ishibashi, J.; Marshall, J.; Maziere, A.; Lovinger, G.; Li, B.; Zakharov, L.; Dargelos, A.; Graciaa, A.; Chrostowska, A.; Liu, S.-Y. *J. Am. Chem. Soc.* **2014**, *136*, 15414−15421.
(63) Yamamoto, K.; Kitsuki, T.; Okamoto, Y. *Bull. Chem. Soc. Jpn.* **1986**, *59*, 1269−1270.
(64) Rudebusch, G. E.; Zafra, J. L.; Jorner, K.; Fukuda, K.; Marshall, J. L.; Arrechea-Marcos, I.; Espejo, G. L.; Ponce Ortiz, R.; Gómez-García, C. J.; Zakharov, L. N.; Nakano, M.; Ottosson, H.; Casado, J.; Haley, M. M. *Nat. Chem.* **2016**, *8*, 753−759.
(65) Yang, X.; Liu, D.; Miao, Q. *Angew. Chem., Int. Ed.* **2014**, *53*, 6786−6790.
(66) Lin, S.-z.; You, T.-p. *Tetrahedron* **2009**, *65*, 1010−1016.
(67) Coulson, C. A.; Daudel, R.; Robertson, J. M. *Proc. R. Soc. London, Ser. A* **1951**, *207*, 306−320.
(68) Rose, B. D.; Sumner, N. J.; Filatov, A. S.; Peters, S. J.; Zakharov, L. N.; Petrukhina, M. A.; Haley, M. M. *J. Am. Chem. Soc.* **2014**, *136*, 9181−9189.
(69) Rudebusch, G. E.; Espejo, G. L.; Zafra, J. L.; Peña-Alvarez, M.; Spisak, S. N.; Fukuda, K.; Wei, Z.; Nakano, M.; Petrukhina, M. A.; Casado, J.; Haley, M. M. *J. Am. Chem. Soc.* **2016**, *138*, 12648−12654.
(70) Gershoni-Poranne, R.; Stanger, A. *Chem. - Eur. J.* **2014**, *20*, 5673−5688.
(71) Rahalkar, A.; Stanger, A. http://schulich.technion.ac.il/Amnon_Stanger.htm.
(72) Stanger, A. *J. Org. Chem.* **2006**, *71*, 883−893.
(73) Frisch, M. J.; Trucks, G. W.; Schlegel, H. B.; Scuseria, G. E.; Robb, M. A.; Cheeseman, J. R.; Scalmani, G.; Barone, V.; Mennucci, B.; Petersson, G. A.; Nakatsuji, H.; Caricato, M.; Li, X.; Hratchian, H. P.; Izmaylov, A. F.; Bloino, J.; Zheng, G.; Sonnenberg, J. L.; Hada, M.; Ehara, M.; Toyota, K.; Fukuda, R.; Hasegawa, J.; Ishida, M.; Nakajima, T.; Honda, Y.; Kitao, O.; Nakai, H.; Vreven, T.; Montgomery, J. A., Jr.; Peralta, J. E.; Ogliaro, F.; Bearpark, M.; Heyd, J. J.; Brothers, E.; Kudin, K. N.; Staroverov, V. N.; Kobayashi, R.; Normand, J.; Raghavachari, K.; Rendell, A.; Burant, J. C.; Iyengar, S. S.; Tomasi, J.; Cossi, M.; Rega, N.; Millam, N. J.; Klene, M.; Knox, J. E.; Cross, J. B.; Bakken, V.; Adamo, C.; Jaramillo, J.; Gomperts, R.; Stratmann, R. E.; Yazyev, O.; Austin, A. J.; Cammi, R.; Pomelli, C.; Ochterski, J. W.; Martin, R. L.; Morokuma, K.; Zakrzewski, V. G.; Voth, G. A.; Salvador, P.; Dannenberg, J. J.; Dapprich, S.; Daniels, A. D.; Farkas, Ö.; Foresman, J. B.; Ortiz, J. V.; Cioslowski, J.; Fox, D. J. *Gaussian 09*, Revision D.01; Gaussian Inc.: Wallingford, CT, 2010.
(74) Parkhurst, R. R.; Swager, T. M. *J. Am. Chem. Soc.* **2012**, *134*, 15351−15356.
(75) Parkhurst, R. R.; Swager, T. M. *Top. Curr. Chem.* **2014**, *350*, 141−175.
(76) Waser, J.; Lu, C. *J. Am. Chem. Soc.* **1944**, *66*, 2035−2042.
(77) Schneebeli, S.; Kamenetska, M.; Foss, F.; Vazquez, H.; Skouta, R.; Hybertsen, M.; Venkataraman, L.; Breslow, R. *Org. Lett.* **2010**, *12*, 4114−4117.
(78) Miljanic, O. S.; Vollhardt, K. P. C. In *Carbon-Rich Compounds: From Molecules to Materials*; Haley, M. M., Tykwinski, R. R., Eds.; Wiley-VCH: Weinheim, Germany, 2006; pp 140−197.
(79) Fukuda, K.; Nagami, T.; Fujiyoshi, J. Y.; Nakano, M. *J. Phys. Chem. A* **2015**, *119*, 10620−10627.
(80) Motomura, S.; Nakano, M.; Fukui, H.; Yoneda, K.; Kubo, T.; Carion, R.; Champagne, B. *Phys. Chem. Chem. Phys.* **2011**, *13*, 20575−20583.

DOI: 10.1021/jacs.6b11397
J. Am. Chem. Soc. 2016, 138, 16827−16838